Chemical Engineering Journal 153 (2009) 1–8

Contents lists available at ScienceDirect

Chemical Engineering Journal

journal homepage: www.elsevier.com/locate/cej

Initial behavior of intraparticle diffusion model used in the description of adsorption kinetics

Feng-Chin Wu [a], Ru-Ling Tseng [b,*], Ruey-Shin Juang [c,d]

[a] Department of Chemical Engineering, National United University, Miao-Li 360, Taiwan
[b] Department of Safety, Health and Environmental Engineering, National United University, No. 1, Lien Da, Kung-Ching Li, Miao-Li 360, Taiwan
[c] Department of Chemical Engineering and Materials Science, Yuan Ze University, Chung-Li 32003, Taiwan
[d] Fuel Cell Center, Yuan Ze University, Chung-Li 32003, Taiwan

ARTICLE INFO

Article history:
Received 14 January 2009
Received in revised form 6 April 2009
Accepted 16 April 2009

Keywords:
Adsorption kinetics
Intraparticle diffusion model
Initial adsorption factor
Activated carbon

ABSTRACT

The intraparticle diffusion model (IPD) proposed by Weber and Morris has been widely applied for the analysis of adsorption kinetics. In this work, the characteristic curves based on this model were plotted with various initial adsorption factors (R_i). Four zones of the initial adsorption according to R_i value from 0 to 1 were classified; that is, approaching completely initial adsorption (zone 4), strongly initial adsorption (zone 3), intermediately initial adsorption (zone 2), and weakly initial adsorption (zone 1). Activated carbons with micropore volume fraction of 0.537 and 0.686 were prepared from oil-palm shells by steam activation. Based on the standard deviations, the kinetics of the adsorption of tannic acid (TA), methylene blue (MB), phenol, and 4-chlorophenol (4-CP) on activated carbons could be best described by intraparticle diffusion model. The initial adsorption of TA and MB belonged to zone 2, and that of phenol and 4-CP mostly belonged to zone 3. Nearly 80% of the 86 adsorption systems surveyed belonged to zones 2 and 3, indicating that the R_i value was smaller when the carbon with smaller particle and steam-activated carbon was used.

© 2009 Published by Elsevier B.V.

1. Introduction

Weber and Morris had presented intraparticle diffusion (IPD) model in 1962 [1,2]. Of the total 57 articles surveyed [3–57], IPD model has been applied in three different forms:

(1) q_t (the amount of adsorption at any time) is plotted against $t^{1/2}$ (the square root of time) to get a straight line that is forced to pass through the origin [3–7];
(2) multi-linearity in q_t vs. $t^{1/2}$ plot is considered (that is, two or three steps are involved to follow the whole process) [8–25]. In this form, the external surface adsorption or instantaneous adsorption occurs in the first step; the second step is the gradual adsorption step, where intraparticle diffusion is controlled; and the third step is the final equilibrium step, where the solute moves slowly from larger pores to micropores causing a slow adsorption rate. The time required for the second step usually depends on the variations of the system (including solute concentration, temperature, and adsorbent particle size), which is difficult to be predicted or controlled;
(3) q_t is plotted against $t^{1/2}$ to obtain a straight line but does not necessarily pass through the origin; that is, there is an intercept [4,26–57]. Almost all the intercepts reported in the literature are positive, indicating that rapid adsorption occurs within a short period of time. To our knowledge, this type of initial adsorption behavior has never been reported.

In this work, the initial adsorption was investigated when IPD model was applied. The intercept of the linearized line was used to define the initial adsorption factor (R_i). The characteristic curves based on IPD model were established with various R_i values. Activated carbons were prepared from oil-palm shells by steam activation for the adsorption of tannic acid (TA), methylene blue (MB), phenol, and 4-chlorophenol (4-CP). The relationships between pore structures of activated carbon, types of solute, and the R_i value were examined. The R_i values of 86 adsorption systems were collected to determine the initial adsorption zone and to analyze the key factors affecting R_i value.

2. Kinetic model

2.1. Characteristic curves and starting factor of IPD model

The fractional approach to equilibrium change is done according to a function of $(Dt/r^2)^{1/2}$, where r is the radius of adsorbent particle

* Corresponding author. Tel.: +886 37 381775; fax: +886 37 333187.
E-mail address: trl@nuu.edu.tw (R.-L. Tseng).

1385-8947/$ – see front matter © 2009 Published by Elsevier B.V.
doi:10.1016/j.cej.2009.04.042

Nomenclature

AC	activated carbon
BTMA	benzyltrimethylammonium
C	constant defined in Eq. (1) (g/kg)
DEDMA	dodecylethyldimethylammonium
D_p	mean pore diameter of adsorbent (nm)
IPD	intraparticle diffusion
k_p	IPD rate constant (mg/(g min$^{1/2}$))
q_e	amount of adsorption at equilibrium (g/kg)
q_{ref}	adsorption amount at time $t = t_{ref}$ (g/kg)
q_t	amount of adsorption at time $t = t$ (g/kg)
R^2	correlation coefficient
R_i	initial factor based on IPD model
S_{ext}	specific area of the adsorbent due to external surface (m^2/g)
S_p	BET specific surface area of the adsorbent (m^2/g)
t	adsorption time (min)
t_{ref}	the longest time in adsorption process (min)
V_{micro}	micropore volume of the adsorbent (cm^3/g)
V_{pore}	total pore volume of the adsorbent (cm^3/g)

and D is the effective diffusivity of solute within the particle. The initial rate of IPD is obtained by linearization of the curve $q_t = f(t^{1/2})$, which is expressed as

$$q_t = k_p t^{1/2} + C \quad (1)$$

where k_p is the IPD rate constant (mg/(g min$^{1/2}$)) and C is a constant for any experiment (mg/g).

For the intercept C, McKay et al. [57] have indicated that "extrapolation of the linear portion of the plot back to the axis provides intercepts which are proportional to the extent of the boundary layer thickness, that is, the larger the intercept the greater the boundary layer effect". This statement has been widely cited by researchers. Their experiment was carried out at different mixing intensities, and the obtained intercepts were negative [57,58]. Thus, they believed that the boundary layer thickness retarded IPD. However, most of the intercepts reported in the literature were positive, that is, there is rapid adsorption in short.

To determine the initial adsorption behavior, the following equations are deduced. First, Eq. (1) can be written as

$$q_{ref} = k_p t_{ref}^{1/2} + C \quad (2)$$

where t_{ref} is the longest time in adsorption process and q_{ref} is the solid phase concentration at time $t = t_{ref}$ for an adsorption system. Subtracting Eq. (2) by Eq. (1), we have

$$q_{ref} - q_t = k_p(t_{ref}^{1/2} - t^{1/2}) \quad (3)$$

Rearrangement of Eq. (3) yields

$$\left(\frac{q_t}{q_{ref}}\right) = 1 - R_i\left[1 - \left(\frac{t}{t_{ref}}\right)^{1/2}\right] \quad (4)$$

where $R_i = (k_p t_{ref}^{1/2}/q_{ref})$, which is defined as the initial adsorption factor of the IPD model.

The so-called characteristic curve based on IPD model can be obtained from Eq. (4). From Eq. (2), R_i is expressed as

$$R_i = \frac{q_{ref} - C}{q_{ref}} = 1 - \left(\frac{C}{q_{ref}}\right) \quad (5)$$

Eq. (5) indicates that R_i can be represented in terms of the ratio of the initial adsorption amount (C) to the final adsorption amount (q_{ref}). When $C = 0$ (i.e., there is no initial adsorption behavior in an adsorption system), $R_i = 1$. In this case, Eq. (2) passes through the origin. This behavior often occurs for synthetic resin adsorbents with large particle sizes and uniform pores [3,4]. When $C = q_{ref}$ (i.e., adsorption occurs right at the beginning of the process), $R_i = 0$. This is not usually regarded as adsorption process but other processes such as aggregation and coagulation, although some powdered adsorbents showed similar phenomena [27,31,51]. The nature of this initial adsorption behavior will be analyzed and explained with the initial characteristic curves based on IPD model.

2.2. Initial characteristic curves and adsorption kinetics

Fig. 1 shows the initial characteristic curves based on IPD model according to Eq. (4) with $R_i = 0.1, 0.5, 0.9$, and 1.0, respectively. When $R_i = 0.1$, the initial point is at $q_t/q_{ref} = 0.9$, which means that the initial adsorption (q_t/q_{ref}) has already reached 90%; later on, the adsorption proceeds following IPD mechanism. On the other hand, the initial point is at $q_t/q_{ref} = 0.5$ when $R_i = 0.5$; i.e., the other 50% of adsorption is governed by IPD. When $R_i = 1.0$, adsorption occurs that is entirely governed by IPD, having a parabola shape curve.

As shown in Table 1, R_i value is divided into four zones: $1 > R_i > 0.9$ is called weakly initial adsorption (zone 1); $0.9 > R_i > 0.5$, intermediately initial adsorption (zone 2); $0.5 > R_i > 0.1$, strongly initial adsorption (zone 3); and $R_i < 0.1$, approaching completely initial adsorption (zone 4). The shapes of adsorption curves based on IPD model are illustrated in Fig. 1. Each adsorption system has its specific characteristic curve. However, the activated carbons with high external surface area and wide pore size distribution often have the same shapes of the initial adsorption curves, as we will discuss in Section 4.3.

3. Materials and methods

3.1. Preparation of the activated carbon

Oil-palm shells were dried at 110 °C overnight. The dried shells were placed in a sealed ceramic oven and heated at a rate of 5 °C/min to 450 °C. At the same time; steam from deionized water in the heated tube was poured into the oven at a rate of 5 cm^3/min for 2 h. Then, steam was quickly removed from the oven through the shells which were thermally decomposed to porous carbonaceous

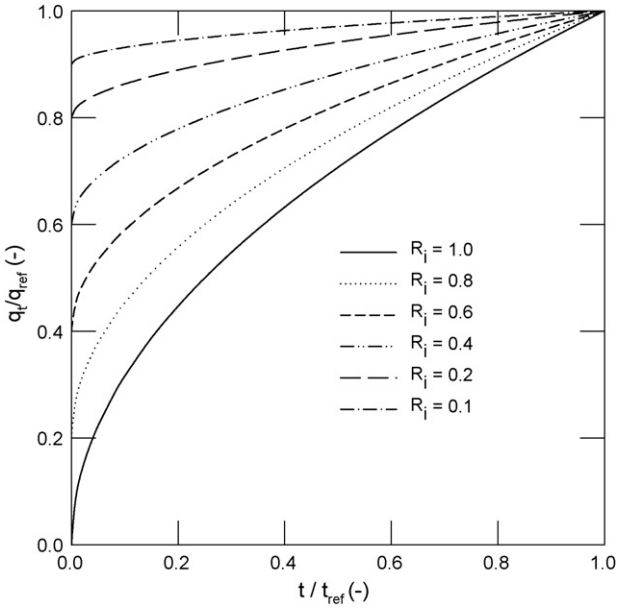

Fig. 1. Adsorption characteristic curves of the dimensionless IPD model (R_i is the initial adsorption factor based on IPD model).

Table 1
Initial adsorption factor (R_i) and kinetic behavior based on IPD model.

R_i	Initial point of kinetic curve (C/q_{ref})	Initial adsorption behavior	Zone
$R_i = 1$	$C/q_{ref} = 0$	No initial adsorption	0
$1 > R_i > 0.9$	$0 < C/q_{ref} < 0.1$	Weakly initial adsorption	1
$0.9 > R_i > 0.5$	$0.1 < C/q_{ref} < 0.5$	Intermediately initial adsorption	2
$0.5 > R_i > 0.1$	$0.5 < C/q_{ref} < 0.9$	Strongly initial adsorption	3
$R_i < 0.1$	$C/q_{ref} > 0.9$	Approaching completely initial adsorption	4

material and a hydrocarbon compound. This is the carbonization step in physical activation process [39].

In the subsequent activation step, the oven was continuously heated at the same rate as above to 900 °C. The flow-rate of steam remained the same. The time of activation was 2, 5, and 6 h, respectively. The final product, activated carbon, was crushed and sieved. Activated carbon with particle sizes of 20–30 mesh (mean size, 715 μm) was screened for the adsorption studies. The steam-activation processes were the same as those described previously [59].

3.2. Measurements of adsorbent properties

The BET surface area of activated carbon (S_p) was measured from the adsorption isotherm of N_2 at 77 K using a sorptiormeter (Porous Materials Inc., BET-202A). Before measurement, the sample was oven-dried at 130 °C overnight and then placed in the sample tube. The tube was heated to 230 °C and then vacuumed for 4 h to a pressure of less than 10^{-4} torr. The total pore volume (V_{pore}) was determined with the manufacturer's software. Moreover, pore size distribution was inferred using the BJH theory [59]. The *t*-plot method was used to calculate the micropore volume (V_{micro}) and the exterior surface area (S_{ext}) [60].

3.3. Procedures for adsorption experiments

Analytical reagent grade methylene blue (MB, Mw (molecular weight) = 284.3 g/mol), tannic acid (TA, Mw = 1701 g/mol), phenol (Mw = 94 g/mol), and 4-chlorophenol (4-CP, Mw = 128.5 g/mol) were purchased from Merck Co. and used as received. Humic acid (HA) was offered from Aldrich Co. The molecular weight of MB did not include the associated chloride ion. The experimental procedures for measuring the adsorption kinetics were the same as those described previously [52,61].

4. Results and discussion

4.1. Physical properties of the activated carbon

In this work, three kinds of activated carbons were prepared from oil-palm shells with an activation time of 2, 5, and 6 h, respectively. The relationship between the volume of N_2 adsorbed and relative pressure (P/P_0) is shown in Fig. 2. It is found that the adsorbed volume increases with increasing activation time. Table 2 lists the BET surface area (S_p), total pore volume (V_{pore}), micropore volume fraction (V_{micro}/V_{pore}), average diameter (D_p), yield (%), and activation time. It is found that 31–46% of the total pore volume is contributed by the pores with a diameter larger than 2 nm.

When the BET surface area and total pore volume are plotted against yield (Fig. 3), S_p and V_{pore} increase with decreasing yield. In order to indicate the effect of activation time on the properties of activated carbon, three kinds of activated carbons, 14.3% AC, 18.5% AC, and 23.7% AC, are designated in terms of the yield.

The external surface area (S_{ext}) of activated carbon is believed to be related to its initial adsorption. Fig. 4 shows the S_{ext} values of activated carbons prepared from corncob [53], plum kernel

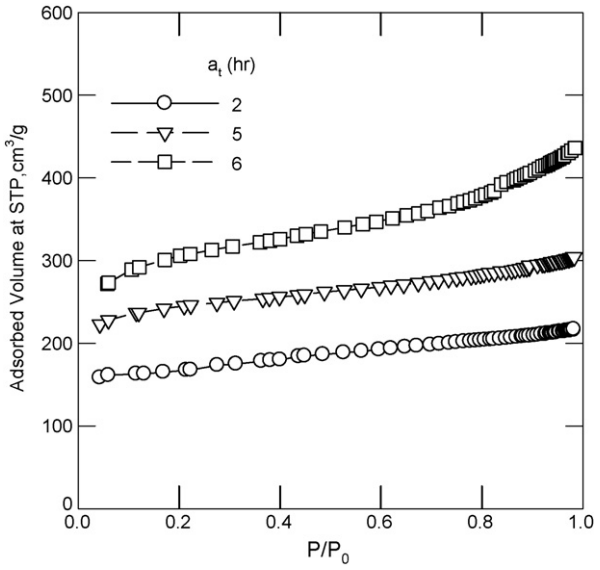

Fig. 2. Adsorption curves of N_2 on oil-palm-shell activated carbons at 77 K.

[33], cane pith [60], and the present oil-palm shells. It is seen that the S_{ext} value of oil-palm-shell carbon is the highest. Especially, the S_{ext} value of 14.3% AC prepared in this work reaches 218 m^2/g. Besides being good for rapid adsorption in wastewater treatment, carbon with a high S_{ext} value is used as supercapacitor, catalyst, and immobilization support for enzymes [62].

4.2. Adsorption kinetics

The linearized plots of q_t vs. $t^{1/2}$ based on IPD model for the adsorption of TA, MB, phenol, and 4-CP on three kinds of activated carbons are shown in Fig. 5. The slopes with three carbons obtained in Fig. 5c and d close, revealing the identical rates of IPD

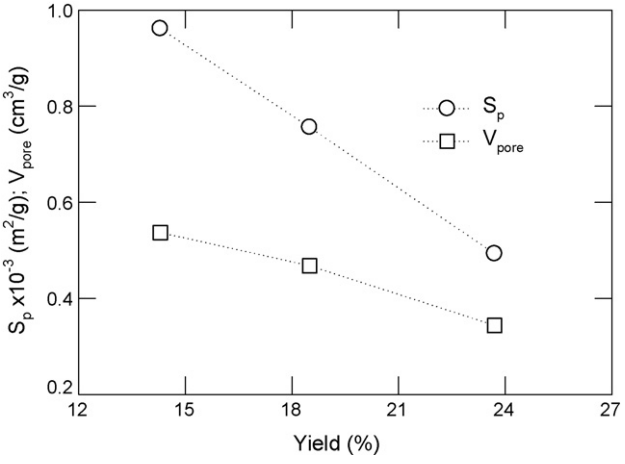

Fig. 3. Relationships between BET surface area (S_p), total pore volume (V_{pore}), and yield of the oil-palm-shell activated carbons.

Table 2
Pore characteristics and yield of the oil-palm-shell activated carbons.

Activation time (h)	S_p (m^2/g)	V_{pore} (cm^3/g)	V_{micro}/V_{pore}	D_p (nm)	Yield (%)
2	493	0.334	0.686	2.71	23.7
5	756	0.468	0.694	2.48	18.5
6	961	0.672	0.537	2.80	14.3

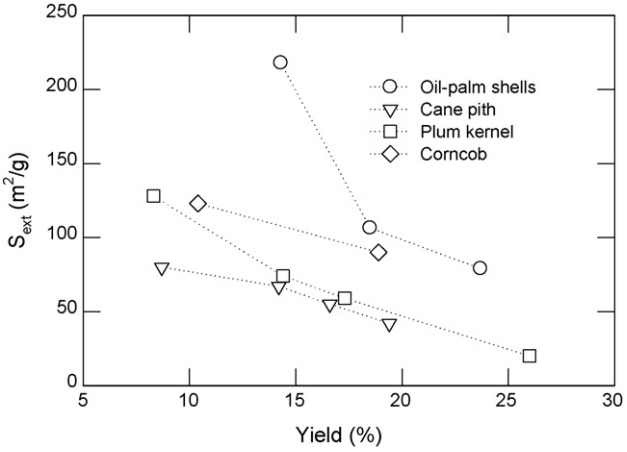

Fig. 4. Relationships between external surface area (S_{ext}) and yield of the activated carbons prepared from various sources.

for the adsorption of small molecules phenol and 4-CP on the carbons. The intercept (C value) increases with decreasing the yield of the carbons, indicating that the carbon with a low yield has a large initial adsorption. Fig. 5a and b shows that the intercept and slope with 23.7% AC are smaller than those with 14.3% AC and 18.5% AC, meaning that the rate of IPD and initial amount of adsorption increase with decreasing the yield of carbon for the adsorption of larger molecules TA and MB. In practice, IPD model is suitable for the description of the present data because the correlation coefficient (R^2) ranges from 0.9892 to 0.9969. None of the straight lines pass through the origin but with a significant intercept. This is because of the wide distribution of pore size for the activated carbons studied.

Table 3 lists the kinetic parameters of IPD model. Another index to evaluate the fitness between the measured and calculated data is the normalized standard deviation (Δq) defined by

$$\Delta q\ (\%) = 100 \times \sqrt{\sum \left[\frac{(q_{t,\mathrm{exp}} - q_{t,\mathrm{cal}})/q_{t,\mathrm{exp}}}{N-1} \right]^2} \quad (6)$$

where the subscripts 'exp' and 'cal' are the experimental and calculated values, respectively, and N is the number of data point. It is evident that the R_i values obtained for the adsorption of phenol and 4-CP are smaller than those of TA and MB. The initial adsorption of TA and MB belongs to zone 2, in the range of intermediately initial adsorption, and that of phenol and 4-CP mostly belongs to zone 3, in the range of strongly initial adsorption.

4.3. Characteristics and distribution of kinetic behavior of the initial adsorption

Actually, the initial adsorption behavior exists in many adsorption processes, but little information is mentioned in the literature.

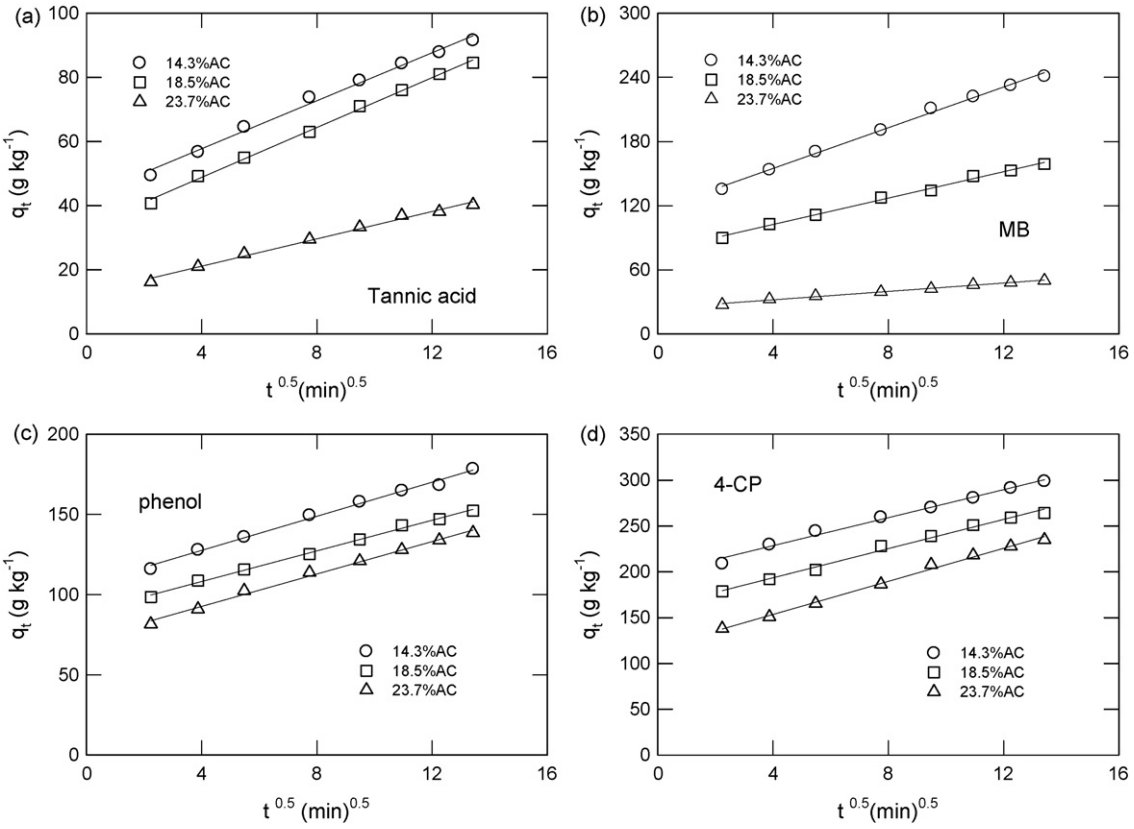

Fig. 5. Analysis of the adsorption kinetics of (a) tannic acid, (b) methylene blue, (c) phenol and (d) 4-CP on oil-palm-shell activated carbons by IPD model.

Table 3
Analysis of the adsorption of various solutes on activated carbons by IPD model.

	Adsorbent	k_p (g/(kg min$^{1/2}$))	C (g/kg)	R_i	Zone	R^2	Δq (%)
TA	14.3% AC	3.74	42.8	0.54	2	0.9923	2.0
	18.5% AC	3.89	33.3	0.61	2	0.9975	1.5
	23.7% AC	2.13	12.6	0.70	2	0.9916	3.2
MB	14.3% AC	9.51	116.7	0.52	2	0.9963	1.3
	18.5% AC	6.16	77.8	0.52	2	0.9951	1.4
	23.7% AC	1.96	24.1	0.52	2	0.9935	2.0
Phenol	14.3% AC	5.32	106.3	0.40	3	0.9929	1.2
	18.5% AC	4.78	89.1	0.42	3	0.9969	0.9
	23.7% AC	5.06	72.5	0.48	3	0.9936	1.6
4-CP	14.3% AC	7.65	197.8	0.34	3	0.9892	1.4
	18.5% AC	7.95	161.7	0.40	3	0.9918	1.3
	23.7% AC	9.03	117.3	0.51	2	0.9953	1.2

Table 4 lists the analysis results of 86 adsorption systems by IPD model together with their longest adsorption time (t_{ref}) and the calculated initial factor (R_i). The R_i values are 1 for Nos. 1–7 in this table, belonging to zone 0 (no initial adsorption), and are $1 > R_i > 0.9$ for Nos. 8–13, belonging to zone 1 (weakly initial adsorption). The above two zones involve the systems using ion exchange resins, silica, chitosan bead, and microporous particle activated carbon as adsorbents in the granular form. The adsorption in these systems occurs under IPD control in almost the whole process.

The R_i values are $0.9 > R_i > 0.5$ for Nos. 14–54, belonging to zone 2 (intermediately initial adsorption), and are $0.5 > R_i > 0.1$ for Nos. 55–81, belonging to zone 3 (strongly initial adsorption). The group of zones 2 and 3 contains 68 systems, the main range of adsorption systems (79%). The adsorbents used in zone 3 mainly include powdered soils (sepiolite, alunite, bentonite, etc.) and the activated carbon with a wider pore size distribution. More than half of the adsorption process has an initial behavior. The R_i values are less than 0.1 for Nos. 82–86, zone 4 (approaching completely initial adsorption), where the initial adsorption occupies more than 90% of the adsorption process.

Generally speaking, key factors affecting R_i values include:

(1) Level of activation of the carbon: for example, burn-off in the systems of Nos. 16, 48, and 67 is 81%, 86%, and 91%, respectively, and the R_i value is 0.89, 0.57, and 0.27. The activation temperatures of Nos. 9 and 26 are 850 and 900 °C, respectively, and the R_i values are 0.94 and 0.78. Moreover, the R_i values for the adsorption of 4-CP on 14.3% AC, 18.5% AC, and 23.7% AC are 0.34, 0.40, and 0.51, respectively. The above results demonstrate that the initial adsorption behavior is more significant (smaller R_i value) at higher burn-off and lower yield (longer activation time).
(2) Particle size of adsorbent: for example, particle size used in the systems of Nos. 9 and 22 are 30–50 mesh and <100 mesh, respectively, and the R_i values are 0.94 and 0.83. Also, particle sizes of Nos. 31 and 35 are 0.505 and 0.335 mm, respectively, and the R_i values are 0.74 and 0.69. The above results reveal that initial adsorption behavior is less significant using adsorbent with a larger particle size.
(3) Activation method of the carbon: for example, the R_i values are 0.67 vs. 0.38, 0.55 vs. 0.23, and 0.85 vs. 0.53 (Nos. 40 vs. 61, 49 vs. 73, and 21 vs. 51), respectively, when the carbons were activated with KOH vs. steam, respectively. Steam activation gives smaller R_i value. This is because KOH activation produces the carbon with fine, uniform pore size, whereas steam activation produces the carbon with wider pore size distribution [61]. That is, steam-activated carbon has a stronger initial adsorption behavior.
(4) Other factors affecting R_i values such as the physicochemical properties of solutes are not discussed here.

4.4. Application of IPD model to adsorption process

Experimental data obtained for the adsorption of four solutes on 14.3% AC and the characteristic curves from Eq. (4) are shown in Fig. 6a. The initial adsorption is smaller for the larger molecules MB and TA, and is larger for the smaller molecules phenol and 4-CP. The possible reason why the initial adsorption of 4-CP is larger than that of phenol is likely related to physicochemical properties of the solute including polarity and solubility. This argument should be further investigated. The experimental data for the adsorption of

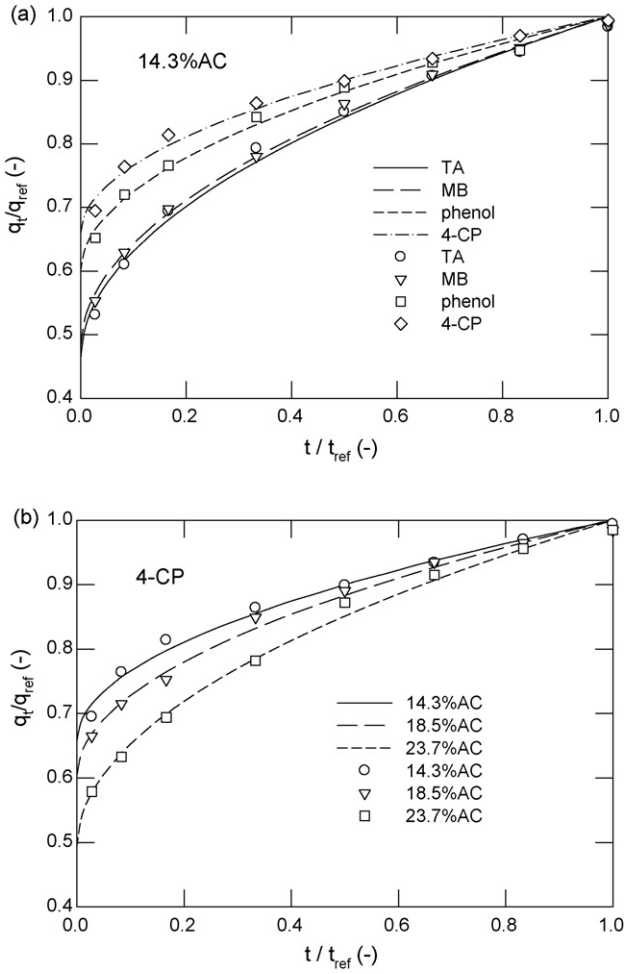

Fig. 6. Dimensionless characteristic curves of the adsorption of (a) TA, MB, phenol, and 4-CP on the carbon with a yield of 14.3% as well as (b) 4-CP on the carbons with a yield of 14.3%, 18.5%, and 23.7%, respectively.

Table 4
Initial adsorption factor (R_i) and kinetic behavior based on IPD model reported in the literature.

No.	Solute	Adsorbent	k_p (g/(kg min$^{1/2}$))	C (g/kg)	t_{ref} (min)	R_i	Ref.
1	Maillard reaction products (MRP)	Adsorption resin	–	0	60	1.0	[3]
2	Dimethyl phthalate	XAD-4	43.7	0	50	1.0	[4]
3	Dimethyl phthalate	NDA-702	25.5	0	36	1.0	[4]
4	Cu(II) (the presence of gluconate)	Chitosan	0.381	0	180	1.0	[5]
5	Cu(II) (the presence of citrate)	Chitosan	0.889	0	90	1.0	[5]
6	Cu(II) (the presence of tartarate)	Chitosan	1.461	0	30	1.0	[5]
7	Effluxes flux dye	Silica	0.87	0	100	1.0	[7]
8	Cu(II) (the presence of EDTA)	Chitosan	1.44	0.612	240	0.973	[38]
9	BR22	Plum-kernel AC (850 °C-activation)	8.76	9	300	0.944	[33]
10	RR222	Cross-linked chitosan bead	11.9	9.83	180	0.942	[55]
11	MB	Dehydrated peanut hull	1.69	3	650	0.935	[37]
12	MB	Jute fiber carbon	3.49	3.16	150	0.931	[43]
13	BB69	Chitosan-encapsulated AC	3.86	5.97	240	0.909	[56]
14	Dimethyl phthalate	NDA-702	22.3	25	100	0.899	[4]
15	Humic acid	Complex beads	3.1	5.71	240	0.894	[46]
16	AB25	Bagasse AC (buff-off, 81%)	3.24	5.78	210	0.890	[26]
17	RR222	Chitosan flakes	3.05	8.38	460	0.886	[54]
18	AB 294	Acid-activated bentonite	10.9	16.0	90	0.866	[29]
19	Cu(II)	Chitosan	1.79	4.51	240	0.860	[38]
20	Cu(II) (the presence of tartaric acid)	Chitosan	2.46	6.39	240	0.856	[38]
21	MB	Fir-wood AC (KOH-activation)	14.78	34.1	180	0.853	[42]
22	MB	Dehydrated peanut hull	5.61	16	200	0.832	[37]
23	Humic acid	Chitosan-encapsulated AC	1.28	4.90	300	0.819	[56]
24	MB	Complex beads	17.2	61.0	240	0.814	[46]
25	RR222	Chitosan bead	11.6	38.8	180	0.800	[55]
26	BR22	Plum-kernel AC (900 °C-activation)	24.1	120	300	0.777	[33]
27	RY145	Chitosan flakes	0.911	5.65	460	0.776	[54]
28	RR222	Complex beads	21.7	116.7	240	0.742	[46]
29	4-CP	Pistachio shells (steam activation)	11.6	43.1	110	0.739	[52]
30	RR222	Chitosan (0.505 mm)	6.00	38.9	330	0.737	[38]
31	RR222	Chitosan beads	6.06	35.5	270	0.737	[54]
32	RB19	Wheat bran	4.20	30.4	400	0.734	[49]
33	BR22	Corncob AC	14.7	80.0	210	0.727	[53]
34	Malachite green	CZn5 (chemical activation with $ZnCl_2$)	16.5	62.9	90	0.713	[47]
35	RR222	Chitosan (0.335 mm)	6.61	53.1	330	0.693	[38]
36	RY145	Wheat bran	3.81	34.8	400	0.686	[49]
37	RR222	Chitosan-encapsulated AC	12.8	90.6	240	0.686	[56]
38	Crystal violet	AC	4.88	17.6	60	0.683	[32]
39	AR 57	Acid-activated bentonite	28.1	127.3	90	0.677	[29]
40	MB	Pistachio-shell AC (KOH activation)	12.5	82.1	180	0.672	[42]
41	MB	Pistachio-shell AC (steam-activation)	8.16	42.3	110	0.669	[52]
42	RY145	Chitosan beads	3.35	30.2	270	0.646	[54]
43	Methylene green	Super absorbent polymer	0.463	2.38	75	0.628	[40]
44	RY145	Chitosan	2.37	27.9	330	0.607	[38]
45	RR195	Wheat bran	2.32	30.2	400	0.606	[49]
46	Cu(II) (the presence of citric acid)	Chitosan	2.46	25.1	240	0.603	[38]
47	Chrome red ME	Fly ash-coal	0.0263	0.198	100	0.57	[6]
48	AB25	Bagasse AC (burn-off, 85.8%)	10.3	113	210	0.569	[26]
49	Phenol	Pistachio-shell AC (KOH activation)	7.43	80.4	180	0.553	[42]
50	RB222	Chitosan	1.09	16.5	330	0.545	[38]
51	MB	Fir-wood AC (steam activation)	10.2	119.4	180	0.534	[42]
52	Cu(II)	Seed of *Capsicum annuum*	0.632	4.38	60	0.528	[34]
53	Phenol	Fir-wood AC (KOH activation)	5.36	65.1	180	0.525	[42]
54	Tannic acid	Complex beads	14.1	218.6	240	0.500	[46]
55	MB	*Euphorbia rigida* AC	6.07	48.3	60	0.493	[50]
56	AR 57	DEDMA-modified sepiolite	17.6	179.2	90	0.482	[28]
57	Malachite green	PETNa8 (polyethyleneterephthalate by chemical activation with NaOH)	7.97	101.9	90	0.426	[47]
58	MB	AC	4.30	48.0	60	0.410	[32]
59	Methylene green	AC	4.72	55.8	60	0.396	[32]
60	Rhodamine B	Super absorbent polymer	1.08	15.1	75	0.382	[40]
61	MB	Pistachio-shell AC (steam activation)	11.1	242.3	180	0.380	[42]
62	BF (Basic Fuchsin)	Super absorbent polymer	0.19	2.7	75	0.379	[40]
63	BG (Brilliant Green)	Super absorbent polymer	0.295	4.8	75	0.347	[40]
65	AB193	Natural sepiolite	0.00164	0.0474	180	0.317	[35]
66	AR57	Calcined-alunite	0.951	20.9	90	0.301	[36]

Table 4 (*Continued*)

No.	Solute	Adsorbent	k_p (g/(kg min$^{1/2}$))	C (g/kg)	t_{ref} (min)	R_i	Ref.
67	AB25	Bagasse AC (burn-off 91.3%)	11.6	406	210	0.293	[26]
68	MB	Super absorbent polymer	0.92	17.1	45	0.265	[40]
69	*o*-Cresol	Pinewood AC	3.97	164.6	210	0.259	[39]
70	BB69	Pinewood AC	10.8	489.5	210	0.242	[39]
71	Safranine T	Super absorbent polymer	0.667	16.4	60	0.240	[40]
72	AB193	BTMA-modified bentonite	7.68	195.7	60	0.233	[30]
73	Phenol	Pistachio-shell AC (steam activation)	2.63	122.6	180	0.230	[42]
74	Crystal violet	Super absorbent polymer	0.203	5.5	60	0.222	[40]
75	Phenol	Fir-wood AC (steam activation)	1.97	101.5	180	0.207	[42]
76	Malachite green	Lignite AC	5.47	163	60	0.206	[41]
77	Cd(II)	Sol–gel + *E. coli*	0.66	42.0	160	0.166	[45]
78	RB19	Surfactant-modified bentonite	0.00314	0.111	40	0.154	[48]
79	AB264	Pinewood AC	9.53	793.5	210	0.148	[39]
80	Phenol	Pinewood AC	1.47	148.8	210	0.125	[39]
81	MB	Nitric-acid treated water-hyacinth	1.21	122.8	200	0.122	[44]
82	Pb(II)	Stevensite	0.443	49.2	120	0.090	[31]
83	3-Chlorophenol	Pinewood AC	1.44	224.1	210	0.085	[39]
84	AB193	DEDMA-modified sepiolite	0.00070	0.101	75	0.057	[27]
85	Cd(II)	Rice polish	0.012	5.0	90	0.022	[51]
86	Cd(II)	Stevensite	0.0433	22.2	120	0.021	[31]

4-CP on 14.3% AC, 18.5% AC, and 23.7% AC and their characteristic curves are given in Fig. 6b, which shows that the initial adsorption increases when the yield decreases.

The relationship between operating time and the amount of adsorption can be obtained from Eq. (4):

$$\left(\frac{t}{t_{ref}}\right) = \left[1 - \frac{1}{R_i}\left(1 - \frac{q_t}{q_{ref}}\right)\right]^2 \quad (7)$$

For an adsorption system, $t/t_{ref} = 0.25$ when $R_i = 0.2$ and $q_t/q_{ref} = 0.9$ as well as $t/t_{ref} = 0.766$ when $R_i = 0.8$ and $q_t/q_{ref} = 0.9$, for instance. Evidently, this equation can be used to determine the adsorption conditions at any time in engineering practice and to select suitable adsorption equipments.

5. Conclusions

A dimensionless initial adsorption equation based on intraparticle diffusion model was deduced and the initial adsorption factor (R_i) was defined. Four zones were classified according to R_i values: weakly initial adsorption, intermediately initial adsorption, strongly initial adsorption, and approaching completely initial adsorption. Of the 86 adsorption systems reported in the literature, the main two zones were the intermediately initial adsorption (48%) and strongly initial adsorption (31%).

Activated carbons with BET surface area from 493 to 961 m^2/g and micropore volume fraction from 0.537 to 0.682 were prepared from oil-palm shells by steam activation. The initial behavior belonged to "intermediately initial adsorption" for the adsorption of TA and MB, whereas mostly belonged to "strongly initial adsorption" for the adsorption of phenol and 4-CP. Literature analysis based on intraparticle diffusion model showed that R_i increased with increasing particle size of the carbon but decreased with increasing activation time. In addition, the R_i value of the carbon by KOH activation was larger than that by steam activation. It is therefore apparent that the initial adsorption concept discussed here is helpful in adsorption engineering design and operation.

Acknowledgment

Financial support of this work by the National Science Council, R.O.C. under contract number NSC 96-2221-E-239-021 is gratefully acknowledged.

References

[1] W.J. Weber, J.C. Morris, Advances in water pollution research: removal of biologically resistant pollutant from waste water by adsorption, in: Proceedings of 1st International Conference on Water Pollution Symposium, vol. 2, Pergamon Press, Oxford, 1962, pp. 231–266.
[2] W.J. Weber, J.C. Morris, Kinetics of adsorption on carbon from solutions, J. Sanit. Eng. Div. Am. Soc. Civ. Eng. 89 (1963) 31–60.
[3] A. Serpen, B. Atac, V. Gokmen, Adsorption of Maillard reaction products from aqueous solutions and sugar syrups using adsorbent resin, J. Food Eng. 82 (2007) 342–350.
[4] W. Zhang, Z. Xu, B. Pan, L. Lu, Q. Zhang, Q. Zhang, W. Du, B. Pan, Q. Zhang, Assessment on the removal of dimethyl phthalate from aqueous phase using a hydrophilic hypercrosslinked polymer resin NDA-702, J. Colloid Interface Sci. 311 (2007) 382–390.
[5] F.C. Wu, R.L. Tseng, R.S. Juang, Role of pH in metal adsorption from aqueous solutions containing chelating agents on chitosan, Ind. Eng. Chem. Res. 38 (1999) 270–275.
[6] G.S. Gupta, G. Prasad, V.N. Singh, Removal of chrome dye from aqueous solutions by mixed adsorbents fly ash and coal, Water Res. 24 (1990) 45–50.
[7] F. Alexander, V.J.P. Poots, G. McKay, Adsorption kinetics and diffusion mass transfer processes during color removal from effluent using silica, Ind. Eng. Chem. Process Des. Dev. 17 (1978) 406–410.
[8] Q. Sun, L. Yang, The adsorption of basic dyes from aqueous solution on modified peat-resin particle, Water Res. 37 (2003) 1535–1544.
[9] E. Lorenc-Grabowska, G. Gryglewicz, Adsorption characteristics of Congo red on coal-based mesoporous activated carbon, Dyes Pigments 74 (2007) 34–40.
[10] S. Wang, H. Li, Kinetic modeling and mechanism of dye adsorption on unburned carbon, Dyes Pigments 72 (2007) 308–314.
[11] Z. Aksu, E. Kabasakal, Batch adsorption of 2,4-dichlorophenoxyacetic acid from aqueous solution by granular activated carbon, Sep. Purif. Technol. 35 (2004) 223–240.
[12] R.R. Sheha, H.H. Someda, Removal of some chelators from aqueous solutions using polymeric ingredients, Chem. Eng. J. 114 (2005) 105–113.
[13] E. Lorenc-Grabowska, G. Gryglewicz, Removal of cyanocobalamine from aqueous solution using mesoporous activated carbon, Dyes Pigments 75 (2007) 136–142.
[14] E. Lorenc-Grabowska, G. Gryglewicz, Adsorption of lignite-derived humic acids on coal-based mesoporous activated carbons, J. Colloid Interface Sci. 284 (2005) 416–423.
[15] J. Ru, H. Liu, J. Qu, A. Wang, R. Dai, Removal of dieldrin from aqueous solution by a novel triolein-embedded composite adsorbent, J. Hazard. Mater. 141 (2007) 61–69.
[16] J.W. Choi, N.C. Choi, S.J. Lee, D.J. Kim, Novel three-stage kinetic model for aqueous benzene adsorption on activated carbon, J. Colloid Interface Sci. 314 (2007) 367–372.
[17] N. Dizge, C. Aydiner, E. Demirbas, M. Kobya, S. Kara, Adsorption of reactive dyes from aqueous solutions by fly ash: kinetic and equilibrium studies, J. Hazard. Mater. 150 (2008) 737–746.
[18] F.C. Wu, R.L. Tseng, R.S. Juang, Preparation of activated carbons form bamboo and their adsorption abilities for dyes and phenol, J. Environ. Sci. Health A 34 (1999) 1753–1776.
[19] R.L. Tseng, F.C. Wu, R.S. Juang, Pore structure and metal adsorption ability of chitosans prepared from fishery wastes, J. Environ. Sci. Health A 34 (1999) 1815–1828.
[20] R.S. Juang, R.L. Tseng, F.C. Wu, S.H. Lee, Liquid-phase adsorption of phenol and its derivatives on activated fibers, Sep. Sci. Technol. 31 (1996) 1915–1931.

[21] F.C. Wu, R.L. Tseng, R.S. Juang, Pore structure and adsorption performance of the activated carbons prepared form plum kernels, J. Hazard. Mater. B 69 (1999) 287–302.
[22] R.L. Tseng, F.C. Wu, R.S. Juang, Effect of complexing agents on liquid-phase adsorption and desorption of copper(II) using chitosan, J. Chem. Technol. Biotechnol. 74 (1999) 533–538.
[23] F.C. Wu, R.L. Tseng, R.S. Juang, Comparative adsorption of metal and dye on flake- and bead-types of chitosans prepared from fishery wastes, J. Hazard. Mater. B 73 (2000) 63–75.
[24] G. McKay, H.S. Blair, J. Gardner, The adsorption of dyes in chitin III. Intraparticle diffusion processes, J. Appl. Polym. Sci. 28 (1983) 1767–1778.
[25] V.V. Sethuraman, B.C. Raymahashay, Color removal by clays kinetic study of adsorption of cationic and anionic dyes, Environ. Sci. Technol. 9 (1975) 1139–1140.
[26] R.S. Juang, F.C. Wu, R.L. Tseng, Characterization and use of activated carbons prepared from bagasse for liquid-phase adsorption, Colloids Surf. A: Physicochem. Eng. Aspects 201 (2002) 191–199.
[27] A. Ozcan, E.M. Oncu, A.S. Ozcan, Adsorption of acid blue 193 from aqueous solutions onto DEDMA-sepiolite, J. Hazard. Mater. 129 (2006) 244–252.
[28] A. Ozcan, A.S. Ozcan, Adsorption of acid red 57 from aqueous solutions onto surfactant-modified sepiolite, J. Hazard. Mater. 125 (2005) 252–259.
[29] A.S. Ozcan, A. Ozcan, Adsorption of acid dyes from aqueous solutions onto acid-activated bentonite, J. Colloid Interface Sci. 276 (2004) 39–46.
[30] A.S. Ozcan, B. Erdem, A. Ozcan, Adsorption of acid blue 193 from aqueous solutions onto BTMA-bentonite, Colloids Surf. A: Physicochem. Eng. Aspects 266 (2005) 73–81.
[31] Y. El Mouzdahir, A. Elmchaouri, R. Mahboub, A. ElAnssari, A. Gil, S.A. Korili, M.A. Vicente, Interaction of stevensite with Cd^{2+} and Pb^{2+} in aqueous dispersions, Appl. Clay Sci. 35 (2007) 47–55.
[32] Y. Onal, Kinetics of adsorption of dyes from aqueous solution using activated carbon prepared from waste apricot, J. Hazard. Mater. 137 (2006) 1719–1728.
[33] R.S. Juang, F.C. Wu, R.L. Tseng, Mechanism of adsorption of dyes and phenols from water using activated carbons prepared from plum kernels, J. Colloid Interface Sci. 227 (2000) 437–444.
[34] A. Ozcan, A.S. Ozcan, S. Tunali, T. Akar, I. Kiran, Determination of the equilibrium, kinetic and thermodynamic parameters of adsorption of copper(II) ions onto seeds of *Capsicum annuum*, J. Hazard. Mater. 124 (2005) 200–208.
[35] A. Ozcan, E.M. Oncu, A.S. Ozcan, Kinetics, isotherm and thermodynamic studies of adsorption of acid blue 193 from aqueous solutions onto natural sepiolite, Colloids Surf. A: Physicochem. Eng. Aspects 277 (2006) 90–97.
[36] S. Tunali, A.S. Ozcan, A. Ozcan, T. Gedikbey, Kinetics and equilibrium studies for the adsorption of acid red 57 from aqueous solutions onto calcined alunite, J. Hazard. Mater. 135 (2006) 141–148.
[37] D. Ozer, G. Dursun, A. Ozer, Methylene blue adsorption from aqueous solution by dehydrated peanut hull, J. Hazard. Mater. 144 (2007) 171–179.
[38] F.C. Wu, R.L. Tseng, R.S. Juang, Kinetic modeling of liquid-phase adsorption of reactive dyes and metal ions on chitosan, Water Res. 35 (2001) 613–618.
[39] R.L. Tseng, F.C. Wu, R.S. Juang, Liquid-phase adsorption of dyes and phenols using pinewood-based activated carbons, Carbon 41 (2003) 487–495.
[40] R. Dhodapkar, N.N. Rao, S.P. Pande, T. Nandy, S. Devotta, Adsorption of cationic dyes on Jalshakti, super absorbent polymer and photocatalytic regeneration of the adsorbent, React. Funct. Polym. 67 (2007) 540–548.
[41] Y. Onal, C. Akmil-Basar, D. Eren, C. Sarici-Ozdemir, T. Depci, Adsorption kinetics of malachite green onto activated carbon prepared from Tuncbilek lignite, J. Hazard. Mater. 128 (2006) 150–157.
[42] F.C. Wu, R.L. Tseng, R.S. Juang, Comparisons of porous and adsorption properties of carbons activated by steam and KOH, J. Colloid Interface Sci. 283 (2005) 49–56.
[43] S. Senthilkumaar, P.R. Varadarajan, K. Porkodi, C.V. Subbhuraam, Adsorption of methylene blue onto jute fiber carbon: kinetics and equilibrium studies, J. Colloid Interface Sci. 284 (2005) 78–82.
[44] M.I. El-Khaiary, Kinetics and mechanism of adsorption of methylene blue from aqueous solution by nitric acid treated water-hyacinth, J. Hazard. Mater. 147 (2007) 28–36.
[45] J.P. Chen, Y.S. Lin, Sol–gel-immobilized recombinant *E. coli* for biosorption of Cd^{2+}, J. Chin. Inst. Chem. Eng. 38 (2007) 235–243.
[46] M.Y. Chang, R.S. Juang, Adsorption of tannic acid, humic acid, and dyes from water using composite of chitosan and activated clay, J. Colloid Interface Sci. 278 (2004) 18–25.
[47] C. Akmil-Basar, Y. Onal, T. Kilicer, D. Eren, Adsorptions of high concentration malachite green by two activated carbons having different porous structures, J. Hazard. Mater. 127 (2005) 73–80.
[48] Y. Onganer, C. Temur, Adsorption dynamics of Fe(III) from aqueous solutions onto activated carbon, J. Colloid Interface Sci. 205 (1998) 241–244.
[49] F. Cicek, D. Ozer, A. Ozer, A. Ozer, Low cost removal of reactive dyes using wheat bran, J. Hazard. Mater. 146 (2007) 408–416.
[50] O. Gercel, A. Ozcan, A.S. Ozcan, H.F. Gercel, Preparation of activated carbon from a renewable bio-plant of *Euphorbia rigida* by H_2SO_4 activation and its adsorption behavior in aqueous solutions, Appl. Surf. Sci. 253 (2007) 4843–4852.
[51] K.K. Singh, R. Rastogi, S.H. Hasan, Removal of cadmium from wastewater using agricultural waste rice polish, J. Hazard. Mater. 121 (2005) 51–58.
[52] F.C. Wu, R.L. Tseng, C.C. Hu, Comparison of properties and adsorption performance of KOH-activated and steam-activated carbons, Micropor. Mesopor. Mater. 80 (2005) 95–106.
[53] F.C. Wu, R.L. Tseng, R.S. Juang, Adsorption of dyes and phenol from water on the activated carbons prepared from corncob wastes, Environ. Technol. 22 (2001) 205–213.
[54] F.C. Wu, R.L. Tseng, R.S. Juang, Enhanced abilities of highly swollen chitosan beads for color removal and tyrosinase immobilization, J. Hazard. Mater. B 81 (2001) 167–177.
[55] R.S. Juang, F.C. Wu, R.L. Tseng, Solute adsorption and enzyme immobilization on chitosan beads prepared from shrimp shell wastes, Bioresour. Technol. 80 (2001) 187–193.
[56] F.C. Wu, R.L. Tseng, R.S. Juang, Adsorption of dyes and humic acid from water using chitosan-encapsulated activated carbon, J. Chem. Technol. Biotechnol. 77 (2002) 1269–1279.
[57] G. McKay, M.S. Otterburn, A.G. Sweeney, The removal of color from effluent using various adsorbents III silica: rate processes, Water Res. 14 (1980) 15–20.
[58] G. McKay, The adsorption of dyestuffs from aqueous solutions using activated carbon. III. Intraparticle diffusion process, J. Chem. Technol. Biotechnol. A 33 (1983) 196–204.
[59] E.P. Barrett, L.G. Joyner, P.P. Halenda, The determination of pore volume and area distributions in porous substances. I. Computations from nitrogen isotherms, J. Am. Chem. Soc. 73 (1951) 373–380.
[60] R.S. Juang, R.L. Tseng, F.C. Wu, Role of microporosity of activated carbons on their adsorption abilities for phenols and dyes, Adsorption 7 (2001) 65–72.
[61] F.C. Wu, R.L. Tseng, R.S. Juang, Preparation of highly microporous carbons from fir wood by KOH activation for adsorption of dyes and phenols from water, Sep. Purif. Technol. 47 (2005) 10–19.
[62] F.C. Wu, R.L. Tseng, C.C. Hu, C.C. Wang, Effects of pore structure and electrolyte on the capacitive characteristics of steam and KOH activated carbons for supercapacitors, J. Power Sources 144 (2005) 302–309.